C³ONTEXT: A Common Consensus on Convective OrgaNizaTion during the EUREC⁴A eXperimenT

Hauke Schulz[1]

[1]Max Planck Institute for Meteorology, Hamburg, Germany

Correspondence: Hauke Schulz (hauke.schulz@mpimet.mpg.de)

Abstract. The C³ONTEXT (A Common Consensus on Convective OrgaNizaTion during the EUREC⁴A eXperimenT) dataset is presented as an overview about the meso-scale cloud patterns identified during the EUREC⁴A field campaign in early 2020. Based on infrared and visible satellite images, 50 researchers of the EUREC⁴A science team manually identified the four prevailing meso-scale patterns of shallow convection observed by Stevens et al. (2020). The common consensus on the observed meso-scale cloud patterns emerging from these manual classifications is presented. It builds the basis for future studies and reduces the subjective nature of these visually defined cloud patterns. This consensus makes it possible to contextualize the measurements of the EUREC⁴A field campaign and interpret them in the meso-scale setting. Commonly used approaches to capture the meso-scale patterns are computed for comparison and show good agreement with the manual classifications. All four patterns as classified by Stevens et al. (2020) were present in January - February 2020 although not all were dominant during the observing period of EUREC⁴A.

The full dataset including postprocessed datasets for easier usage are openly available at the Zenodo archive at https://doi.org/10.5281/zenodo.5724585 (Schulz, 2021b).

1 Introduction

Clouds are often clustered. Examples of larger clusters are squall lines and the intertropical convergence zone. But also much smaller clouds like shallow trade wind cumuli, are often seen clustered on a scale of several hundred kilometers. The understanding of these meso-scale patterns of shallow convection is still sparse. However, the ubiquity of these clouds and their reoccurring structure suggest that they play an important role in determining the radiative effects of the trade-wind regimes (Bony et al., 2020). The ElUcidating the RolE of Cloud-Circulation Coupling in ClimAte (EUREC⁴A) field campaign addresses among others, the question of which processes are at play that change the meso-scale appearance of shallow convection. Prior to the campaign, studies concentrated on the classification of meso-scale patterns based on satellite images by visual inspection (Stevens et al., 2020), rule-based algorithms (Bony et al., 2020) or trained neural networks (Rasp et al., 2020). Common to all of these methods is their focus on four specific meso-scale cloud patterns that have been identified as commonly occuring in the North Atlantic downwind trades (Stevens et al., 2020). An overview about these four patterns which are named by their visual impressions as *Sugar*, *Gravel*, *Flowers* and *Fish* is given in Fig. 1.
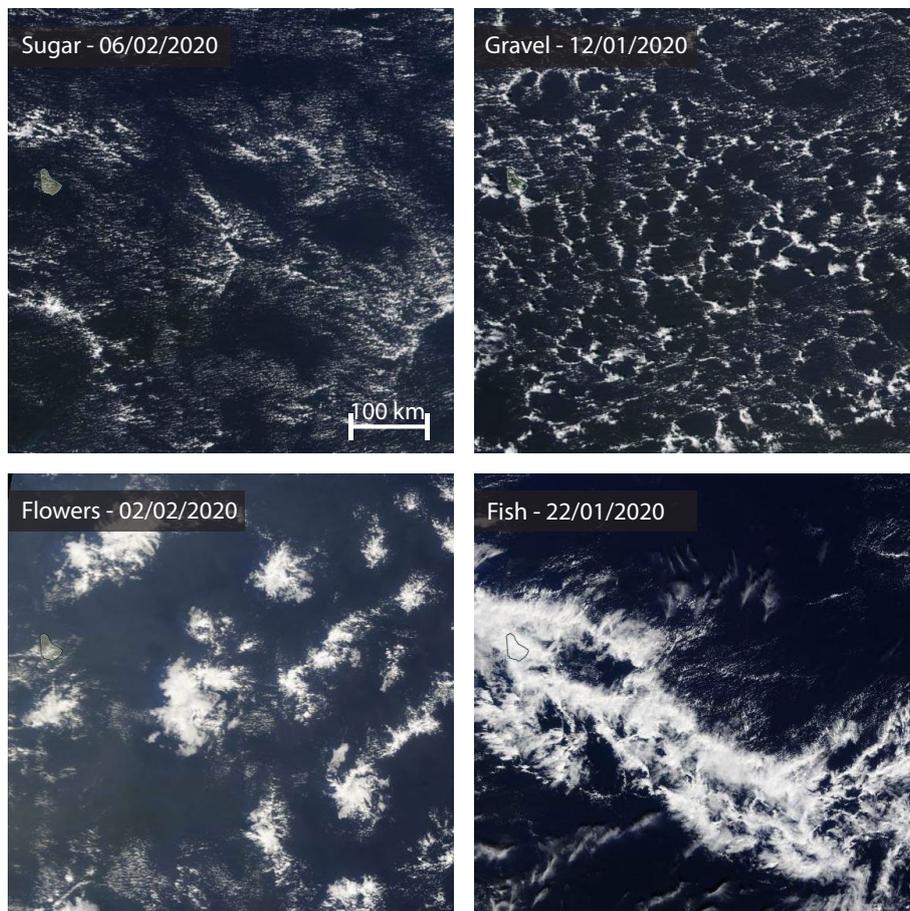
Figure 1. Four classes of meso-scale patterns of shallow convection have been labeled by 50 scientists in satellite images of January and February 2020. An example of each of these classes is shown based on the reflectance measurements of the Moderate Resolution Imaging Spectroradiometer (MODIS) onboard the TERRA satellite (Sugar, Gravel) and the Visible Infrared Imaging Radiometer Suite (VIIRS) onboard Suomi NPP satellite (Flowers, Fish). Example images provided by NASA Worldview.

25   These efforts show that the categorization of the meso-scale patterns is an elementary step in acquiring further knowledge about the cloud processes in the downstream trades. 50 scientists from 15 research institutes who were involved in the EUREC[4]A field campaign in January - February 2020 therefore participated in a joint online classification event. The results of this classification event are presented here. Due to the high attendance, the presented dataset can be interpreted as the common judgement of the EUREC[4]A science team on the meso-scale patterns of shallow convection in the trades during EUREC[4]A.

30   This dataset therefore allows to consistently communicate about the otherwise subjectively defined patterns and puts the measurements taken during EUREC[4]A in their meso-scale context to advance the process understanding of shallow convection in the trades.

The paper is structured as follows: the dataset and its collection are described in Section 2. Potential use cases are described
35   in Section 3. In Section 4 additional classification methods that are able to detect the four meso-scale patterns are applied to
the EUREC[4]A time period and compared to the manual classifications described in this paper. We conclude with Section 5.

2   Data description and development

The manual classifications were gathered through the online platform zooniverse.org which has already been successfully used
in an earlier project by Rasp et al. (2020). The platform makes it possible to crowd-source labels for e.g. machine learning
40   projects. Additional workflows can be defined to separate different image sources or to separate, for example, labels made
during a practice run from those that belong to the actual classification. The former allowed everyone to familiarize with the
zooniverse.org platform without influencing the results.

For this dataset, we defined three workflows. Two workflows are based on satellite observations in the visible (EUREC[4]A VIS)
and infrared channels (EUREC[4]A IR) made by both the Geostationary Operational Environmental Satellite 16 (GOES-16)
45   Advanced Baseline Imager (ABI) and Moderate Resolution Imaging Spectroradiometer (MODIS) in the first and only ABI in
the latter case. Another workflow (EUREC[4]A ICON) is based on a storm-resolving simulation covering the EUREC[4]A time
period. This workflow has been included to test how well a storm-resolving simulation is able to reproduce the patterns. Here
we used output from an ICOsahedral Nonhydrostatic (ICON) simulation with a grid-spacing of $1.25\,\mathrm{km}$ that was initialized
daily by the ECMWF IFS and forced hourly. Each run is 48 hours long. The first 24 hours were discarded to allow for spin-up.
50   To visualize the simulation output, we calculated a pseudo-albedo α by following the approximation of Zhang et al. (2005):

$$\tau \;\; = \;\; 0.19 \cdot \mathrm{LWP}^{\frac{5}{6}} \cdot N^{\frac{1}{3}} \tag{1}$$

$$\alpha \;\; = \;\; \frac{\tau}{6.8 + \tau}, \tag{2}$$

where τ is the optical depth, LWP is the liquid water vapor path and N an assumed cloud droplet number density. Here a
number density of $70\,\mathrm{cm}^{-3}$ is used, which is at the lower end of the observed concentrations (Siebert et al., 2013).
55   All workflows are further described in Tab. 1.

On March 24, 2020 the international, virtual classification event was hosted with 51 scientists from 15 institutes participating
to create the pattern classifications. For a full day the participants classified patterns of shallow trade-wind convection by
labeling, i.e. drawing rectangles around the four common types: *Sugar*, *Gravel*, *Flowers* and *Fish* (Stevens et al., 2020).

In the end, over 12,500 labels were gathered and accumulated intentionally on the workflows with observations (see Fig. 2) as
60   it quickly turned out that the identification of the patterns in the model simulation was too demanding. The features had too
little similarity with those found in nature. The daily composites shown in Figure A11 reveal that *Sugar* was particularly hard
to identify. *Fish* and *Flowers* however, were often classified at the same days as in the observational workflows (EUREC[4]A
VIS, EUREC[4]A IR). This is also reflected by the comparison of the amount of labels that has been created for each class and
workflow (Fig. 2). *Sugar* has been classified least in the simulation workflow, while the largest feature, *Fish*, however, has been

Table 1. Description of data sources used to create the images of the classification workflows.

	EUREC^{4}A VIS		EUREC^{4}A IR	EUREC^{4}A ICON
	MODIS (TERRA/AQUA)	ABI (GOES-16)	ABI (GOES-16)	
Domain	5-20 N; 62 - 40 W			5 - 20 N; 62 - 44 W
Period	07.01.2020 - 22.02.2020			16.01.2020 - 20.02.2020
Resolution (shown)	~1 km			~2 km
	2-hourly, 12-20 UTC	2-hourly		2-hourly
Data source	Corrected reflectance	Channel 02 (red)	Channel 13 (IR)	pseudo-albedo
Number of scenes	94	234	562	425
Remarks				Data shown after 24 hours spin-up
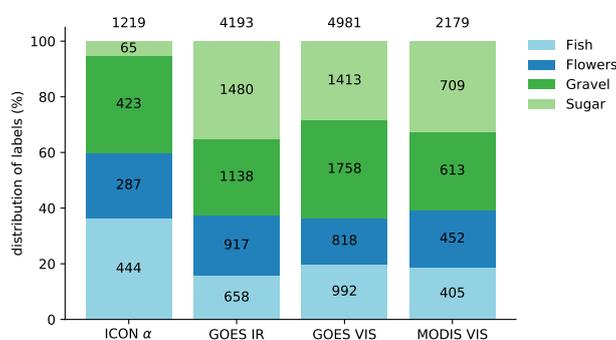
Figure 2. Distribution of labels by data source. The relative distribution is shown at the y-axis, while the absolute number of labels is indicated within each bar. The total number of labels per workflow is shown at the top of each bar.

identified more often. This supports the assumption that larger features are better reproduced in storm-resolving simulations than features of smaller scales, like *Sugar*.

Because all users have familiarity with the patterns either by previous work and/or being involved in the classification event of Rasp et al. (2020) it can be assumed that the labels are of high quality. In addition, they were trained immediately before starting the classification through an online presentation to get familiar with the labeling interface on zooniverse.org and to refresh once more the different meso-scale cloud pattern categories. Compared to Rasp et al. (2020) where the focus has been to classify as many diverse cloud scenes as possible to capture the variability and thus serve as a better machine learning dataset, the aim for this dataset is to create a common classification dataset for the EUREC^{4}A time period that participating scientists agree on and can directly be used in further studies. Therefore, the temporal frequency has been increased from daily cloud

scenes to 2-hourly cloud scenes to reflect also the changes on the sub-daily scale such as those identified by Vial et al. (2021).

75 Due to this design difference, a single day is now on average classified 20 times in case of the visible workflow instead of just about 6 (3 per daytime AQUA/TERRA satellite overpass) as in Rasp et al. (2020). Each individual cloud scene is however still viewed about three times.
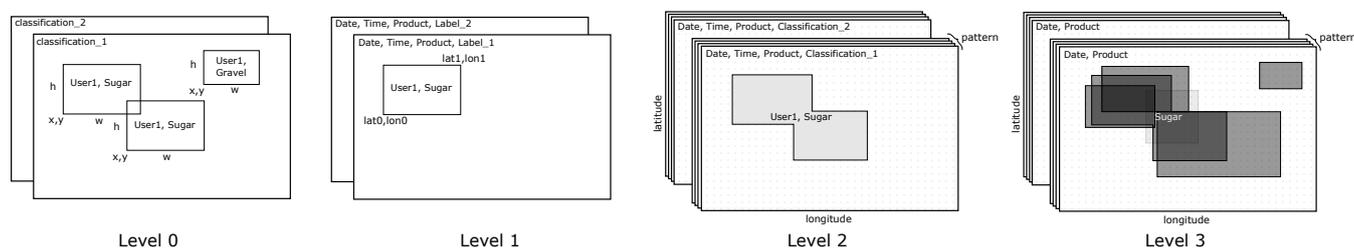
Figure 3. Overview of processing levels of the datasets including the variable names used in the respective datasets.

After the joint classification event, over 12,500 labels were processed to make them more user friendly, especially because

80 the raw data misses any temporal and geospatial information. The processing steps with the intermediate products are illustrated in Fig. 3 and described as follows:

- *Level 0*

  The *Level 0* dataset consists of the raw data output and originate from the zooniverse platform. It consists of CSV files that contain entries for each workflow, image (subject) and classification including technical details like the time spent

85 on drawing a specific label. Labels are given by their origin (x,y) and their height (h) and width (w) given in pixel coordinates.

- *Level 1*

  The *Level 1* dataset is further processed and combines the information distributed over the *Level 0* dataset files. It contains each label as a separate entry and contains information about the classified object, the user and the geographical

90 and Cartesian coordinates of the label. This product is saved in a netCDF file.

- *Level 2*

  For the *Level 2* dataset, the data are merged by `classification_id`.
  The `classification_id` is a unique identifier of a classification, where a classification refers here to the process of labeling a single image by a single user. The user might use several labels of the same or different kind to completely

95 classify a scene. This process eliminates overlaps of same-user classifications for each pattern and turns the data into masks, rather than coordinates (see Fig. 3). Masks have the advantage to be easier queried whether a specific location is influenced by a meso-scale pattern or not. This product is saved in zarr.

– *Level 3*

To ease working with the dataset, the percentage of agreement (p) among users on a specific pattern on each location is
100   calculated and saved as `Level 3` data for each workflow. It is calculated as follows:

$$p_{\mathrm{pattern}}(i,j) = \frac{\sum_0^U c(i,j)}{U}, \tag{3}$$

where U is the number of users that have seen the particular image, c the classification mask from the *Level 2* data and
i,j the geographic coordinates. Because the labels of users that attributed several classes to one pixel are not removed,
$\sum p$ can be greater than 100%.

105   An example of the daily average of this agreement is shown in Fig. 4 and shown for each day and workflow in Appendix
A to give an impression of the dataset and in particular the presence and distribution of meso-scale patterns during the
EUREC⁴A field campaign. This product is saved in zarr.
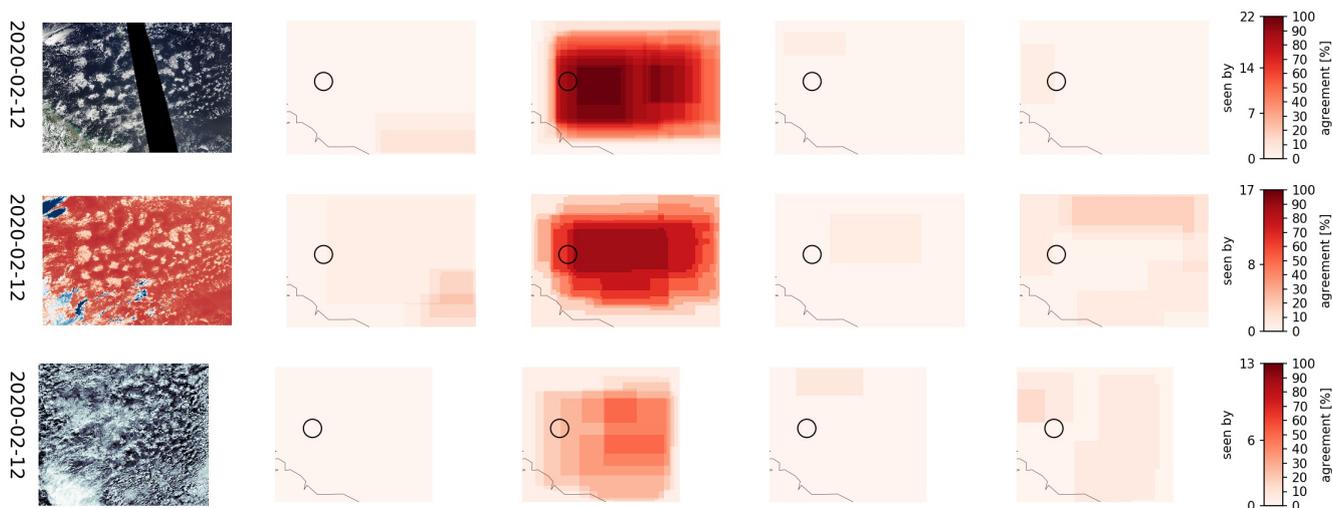
Figure 4. Manual classification examples for the three workflows (top to bottom: visible, infrared, simulation. The labels for each pattern
(from left to right: *Sugar*, *Flowers*, *Fish*, *Gravel*) are shown next to the labeled image. Coastline of South America is marked in black. The
circle marks the EUREC⁴A circle, one focus area of the EUREC⁴A field campaign and the main flight pattern of the participating research
aircraft HALO (Konow et al., 2021). Coastlines are based on GSHHG shapefiles (Wessel and Smith, 1996).

3   Potential dataset use and reuse

The EUREC⁴A field campaign has been an international study with a wide range of research platforms and many minor
110   objectives (Stevens et al., 2021). This dataset does not only cover the core area of the experiment, but also the wider area
and time period. While the participating research airplanes and drones were mostly staying in the trade-winds, some research
vessels conducted measurements as far south as 6.5°N.

This dataset gives the opportunity to study all these measurements in the context of the meso-scale patterns observed in the downwind trades. Due to the high subjectivity of these meso-scale cloud pattern definitions, it is of particular importance
115 to discuss results based on a common consensus to keep studies comparable. The C³ONTEXT dataset can serve as such a reference for the period of the EUREC⁴A field campaign.

Fig. 5 shows the meso-scale context for the three platforms participating in EUREC⁴A. Based on the classifications of the infrared workflow, the daily changes in the cloud patterns become visible. Before the intense observation period (IOP), January 20th to February 20th, the prevailing cloud pattern at the Barbados Cloud Observatory has been *Gravel*. With the start of the
120 IOP, *Fish* has been detected most in the research area. After January 24, patterns were much less widespread and well defined, such that more disagreement on the pattern exists. This development is independent of the location. Both the platforms in the north as well as the R/V Atalante, which sailed further south in the *Boulevard de Tourbillons*m which is defined by Stevens et al. (2021) as the area of the coastline of Brazil where the North Brazil Current (NBC) Rings occur. The few classifications towards the end of the IOP around February 15th are caused by mid-level clouds obscuring the view on the shallow convection.
125 In Appendix A the level 3 products are visualized for each studied day and can be used as a look-up table to quickly identify if a pattern has been identified at a specific time and place.
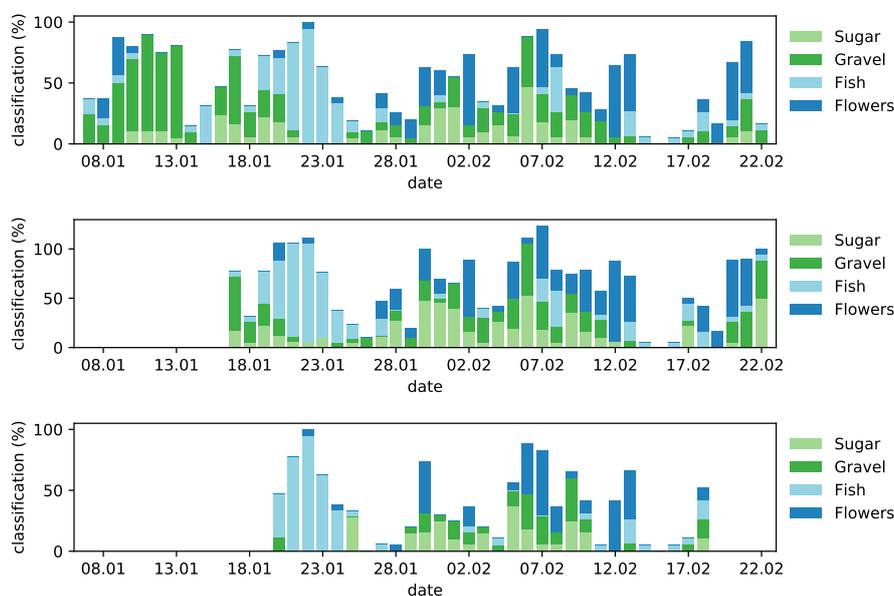
Figure 5. Exemplary use cases: meso-scale setting of research platforms during EUREC⁴A (top to bottom: Barbados Cloud Observatory (BCO), R/V Meteor, R/V Atalante)

4   Comparison with other classifications

Several methods have been developed to describe the meso-scale structure of shallow convection (Wood and Hartmann (2006); Rasp et al. (2020); Bony et al. (2020); Denby (2020)). Here we focus on the two methods that aim specifically to detect the
130   four meso-scale patterns of the downwind trades as defined by Stevens et al. (2020) and shown in Fig. 1. Bony et al. (2020) combined a measure of organization (I_{org}, Tompkins Adrian M. and Semie Addisu G. (2017)) with the mean cluster size (S), while Rasp et al. (2020) developed a deep neural network to detect the patterns.

To assess the agreement between the different classification methods we compare the method of Bony et al. (2020) and a deep neural network based on Rasp et al. (2020) but which is able to detect the patterns in geostationary infrared images of
135   GOES-16 ABI (Schulz et al., 2021) instead of visible images taken onboard the polar-orbiting satellites TERRA and AQUA.

Because the I_{org}/S measure is sensitive to the domain size, we focus on a domain size of 10×10 degrees to do the comparison. Precisely, we focus on the region $10°$N - $15°$N and $58°$W - $48°$W. This domain size ensures that the I_{org} is describing the organization on the meso-scale rather than on a different spatial scale. The method has been successfully used in this domain in Bony et al. (2020) and applied accordingly. Brightness temperatures between $280\,\mathrm{K}$ and $290\,\mathrm{K}$ are regarded as clouds. Days
140   where the 25th percentile of brightness temperatures within any satellite image is lower than $285\,\mathrm{K}$ are discarded to avoid a bias by high clouds.
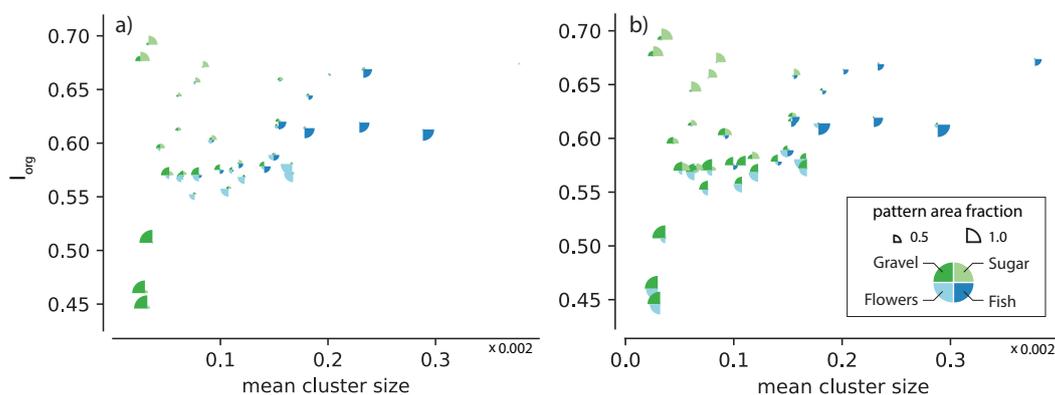
Figure 6. Comparison of the I_{org} *versus mean cluster size (S)* classification method and the (a) *manually* classified patterns and (b) the neural network classifications. For each I_{org}/S classification, the manually/automatically classified pattern area for each pattern is indicated as wedges of different size. All classifications are based on the GOES-16 ABI infrared images and are daily averages.

Fig. 6 shows the comparison of the different methods. We recognize in Fig. 6 that the I_{org} distribution has a large range of values for small mean cluster sizes and narrows with increasing mean cluster size. This is in agreement with Bony et al. (2020). From the appearance of the patterns, we expect *Gravel* and *Flowers* to be rather regularly distributed and therefore to
145   have a lower I_{org} compared to *Fish* and *Sugar*. It should be noted that the I_{org} is calculated based on a threshold in brightness temperature and therefore only the deeper clouds in the *Sugar* field are detected leading to a higher I_{org} than one would expect

from a rather randomly distributed cloud field. The mean cluster size should be small for *Sugar* and *Gravel* and larger for *Flowers* and *Fish*.

150   Indeed, the pattern area fraction maximizes for each pattern in the respective quadrant of the I_{org}/S space independent of the classification method. *Gravel* classifications dominate the lower left quadrant, *Sugar* dominates the upper left quadrant and *Fish* the upper right one. *Flowers* are harder to associate with a quadrant as they are more centered. This is also in alignment with Bony et al. (2020) where the lower right quadrant includes not only *Flowers* but also about 35% of the *Fish* cases (their Fig. 1c).
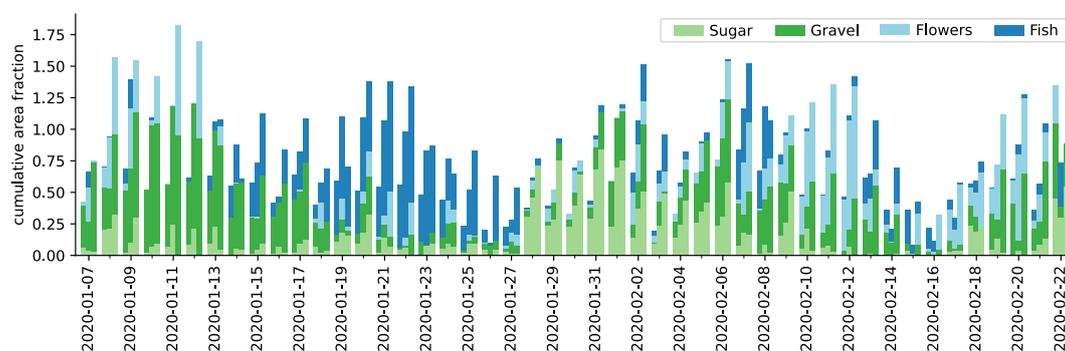
Figure 7. Time series of area fraction covered by each pattern as identified in the workflows EUREC⁴A VIS (left bar), EUREC⁴A IR (center bar) and the deep neural network (right bar) within the area of 10°N - 15°N and 58°W - 48°W.

Fig. 7 reveals the time series of the area fraction covered by the meso-scale patterns within the region of 10°N - 15°N and 155   58°W - 48°W. To convert the label frequencies of the *level 3* dataset to an actual classification, we applied a threshold of 0.1 on the frequencies. Frequencies lower than this threshold are not considered as consensus and are handled as unclassified regions. Fig. 7 shows that in January - February 2020 all patterns were dominant at least once. It also shows that the day-to-day variability in changes of the dominant pattern type are rather rare and a rather smooth transition from *Gravel* to *Fish* to *Sugar* to *Flowers* is observed.

160   Overall, the different classification methods agree well with each other and no large discrepancies are found. This reassures that these methods are valid for further analysis of meso-scale patterns. While the I_{org}/S metric is computationally cheap and can be easily applied to different regions, the manual classifications are naturally more accurate. The neural network approach is a good compromise between precision and scalability. However, when concentrating on a limited time period like the EUREC⁴A field campaign period where each pattern is only occurring a few times, manual classifications are most 165   accurate.

5   Conclusions

Meso-scale patterns of shallow convection are a main focus of the EUREC[4]A field campaign that took place in January and February 2020. To gain a better process understanding of shallow convection in the trades, the classifications of meso-scale patterns offer the opportunity to study the measurements in their meso-scale context and thereby split the observations into less
170   complex pieces and disentangle otherwise superimposed processes. Here, we present C[3]ONTEXT, a dataset on the common consensus on the meso-scale patterns which occurred during the broader EUREC[4]A time period and emerges from the manual classifications done by members of the EUREC[4]A science team.

C[3]ONTEXT reveals, that all patterns are observed during the studied period of January and February 2020. However, in the intense observation period of the EUREC[4]A field campaign, January 20th to February 20th, *Gravel* is only sporadically
175   identified and not prevalent in the study area. In contrast, a week before the intense observation period, *Gravel* is the most dominating pattern in the research area. Instruments that were already running at this time, like those at the Barbados Cloud Observatory, were able to gain measurements under the meso-scale influence of *Gravel* and complement the measurements from the IOP.

The difficulties of the participants to classify the patterns in the output of a storm-resolving simulation demands further
180   investigations on how well simulations can capture the variability of meso-scale patterns of shallow convection in the trades.

A comparison of the manual classification approach with other methods used in the literature to identify the four meso-scale patterns of shallow convection reveals a generally good agreement and confirms the validity of the different approaches. Nevertheless, the manual classifications are beneficial for limited temporal and spatial studies especially when the classifications are done by a group of several trained scientists. It presents a way to gain a consensus of subjectively defined cloud patterns
185   without an additional layer of complexity from a neural network or any other algorithm.

In general, it has been shown that with little effort, classifications of the cloud field are possible and can be a huge benefit for the community, encouraging this approach for future studies.

6   Code and data availability

The C[3]ONTEXT dataset including raw data is openly available at the zenodo database (European Organization For Nuclear
190   Research and OpenAIRE, 2013): https://doi.org/10.5281/zenodo.5724585 (Schulz, 2021b). The source code necessary to generate the dataset is available at https://doi.org/10.5281/zenodo.5724762 (Schulz, 2021a) together with examples on how to process the data and retrieve the classifications for any platform as shown in e.g. Fig. 5.

Appendix A: Daily classification overview

Competing interests.   The author declares that he has no conflict of interest.
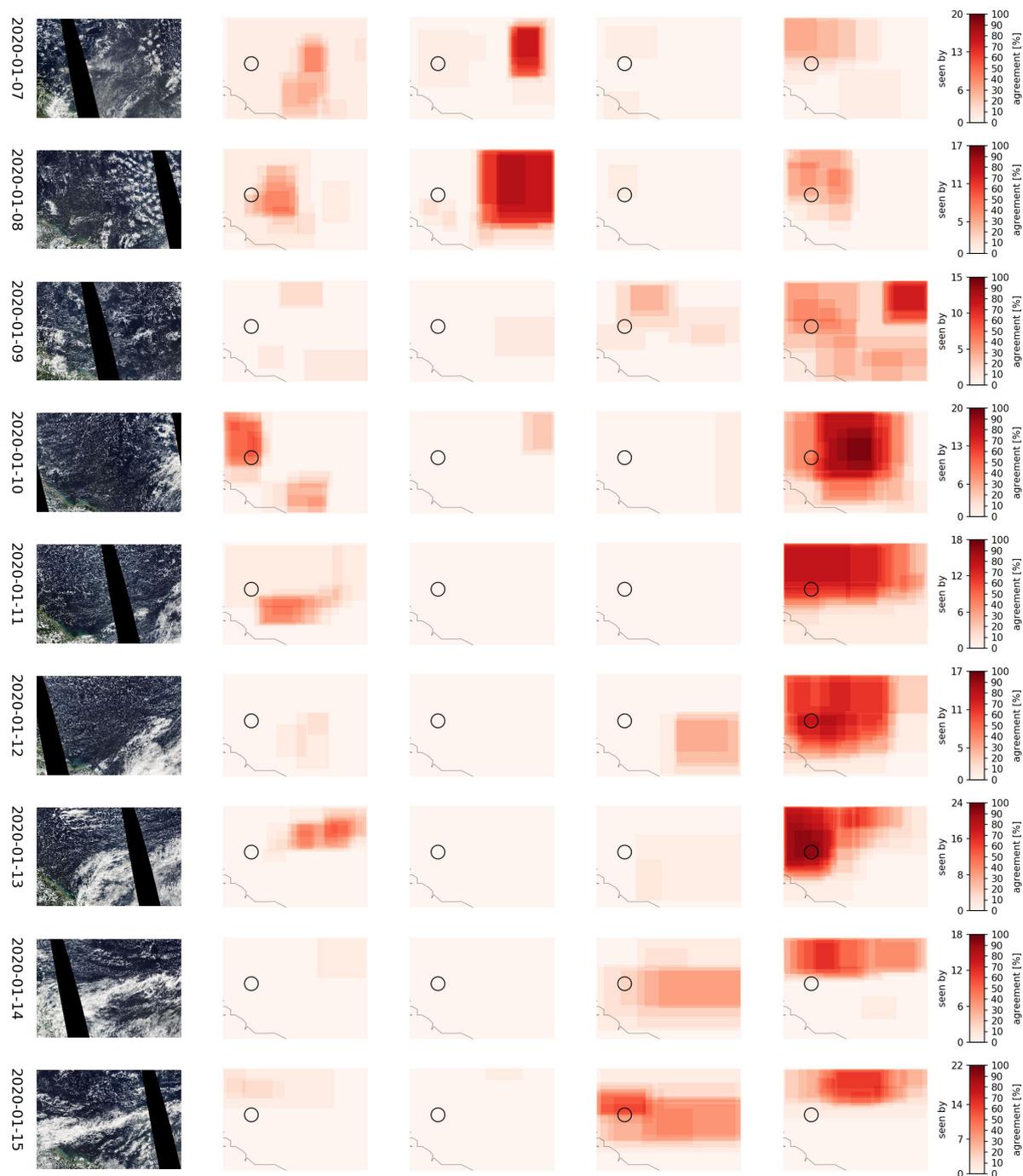
Figure A1. Heatmaps of manual classifications based on MODIS (Aqua and Terra) visible imagery. Left to right: Visible imagery during Aqua overpass, User agreement on *Sugar*, *Flowers*, *Fish* and *Gravel* (left to right). The circle marks one focus area of the EUREC[4]A field campaign and the main flight pattern of the participating research aircraft HALO Konow et al. (2021). Coastlines are based on GSHHG shapefiles (Wessel and Smith, 1996).

Open Access Earth System Discussions
Science
Data
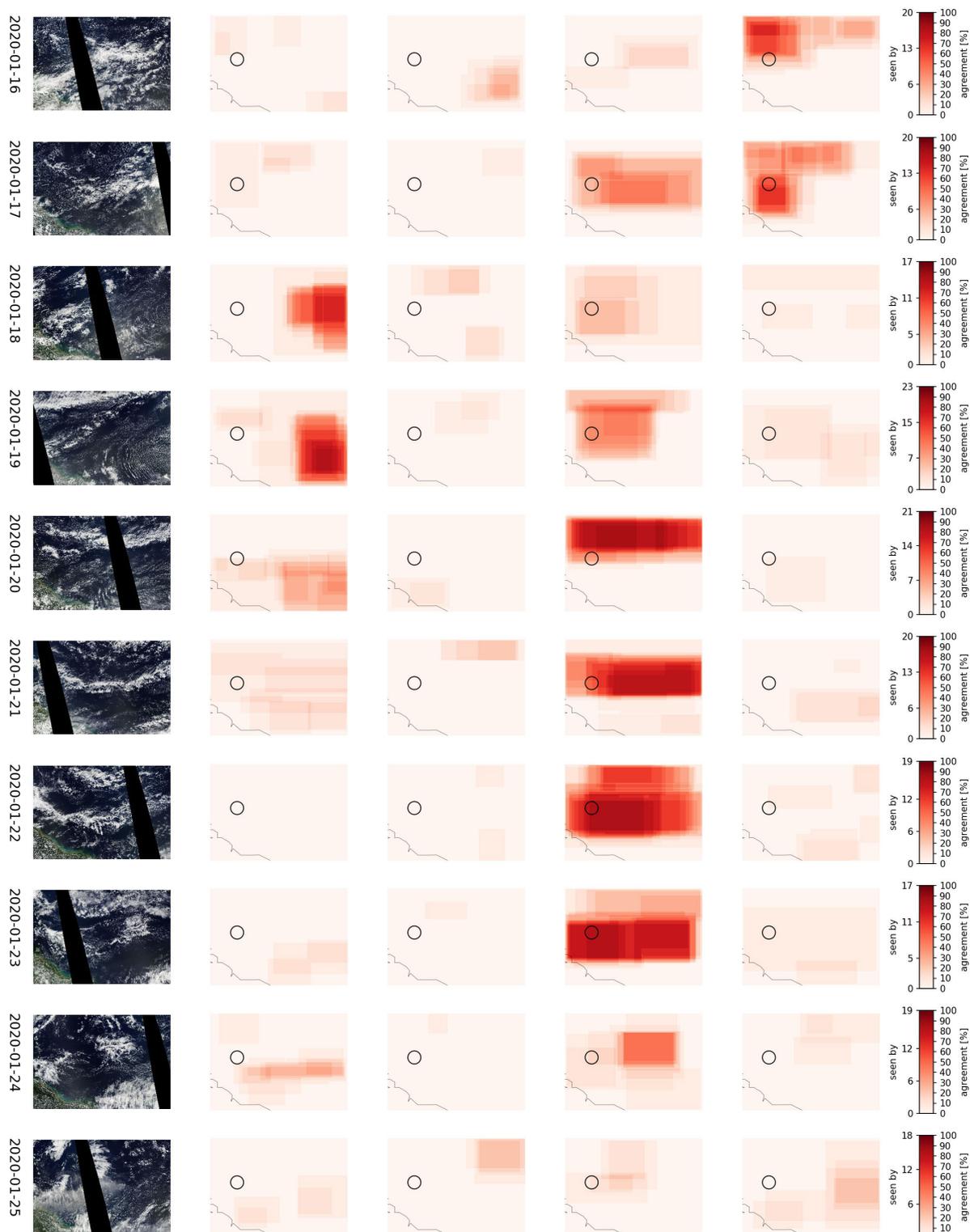
Figure A2. Continuation of Fig. A1
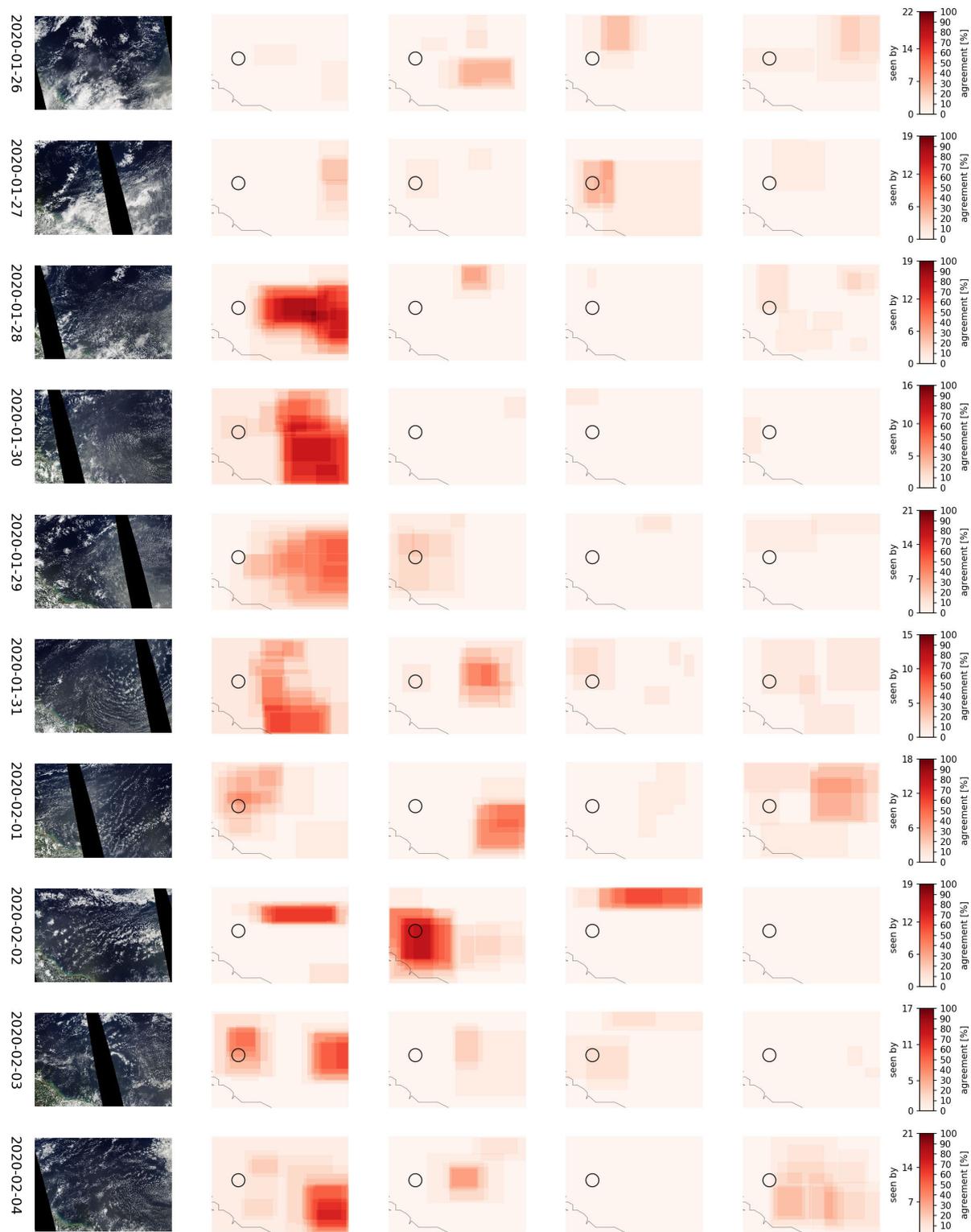
Figure A3. Continuation of Fig. A2
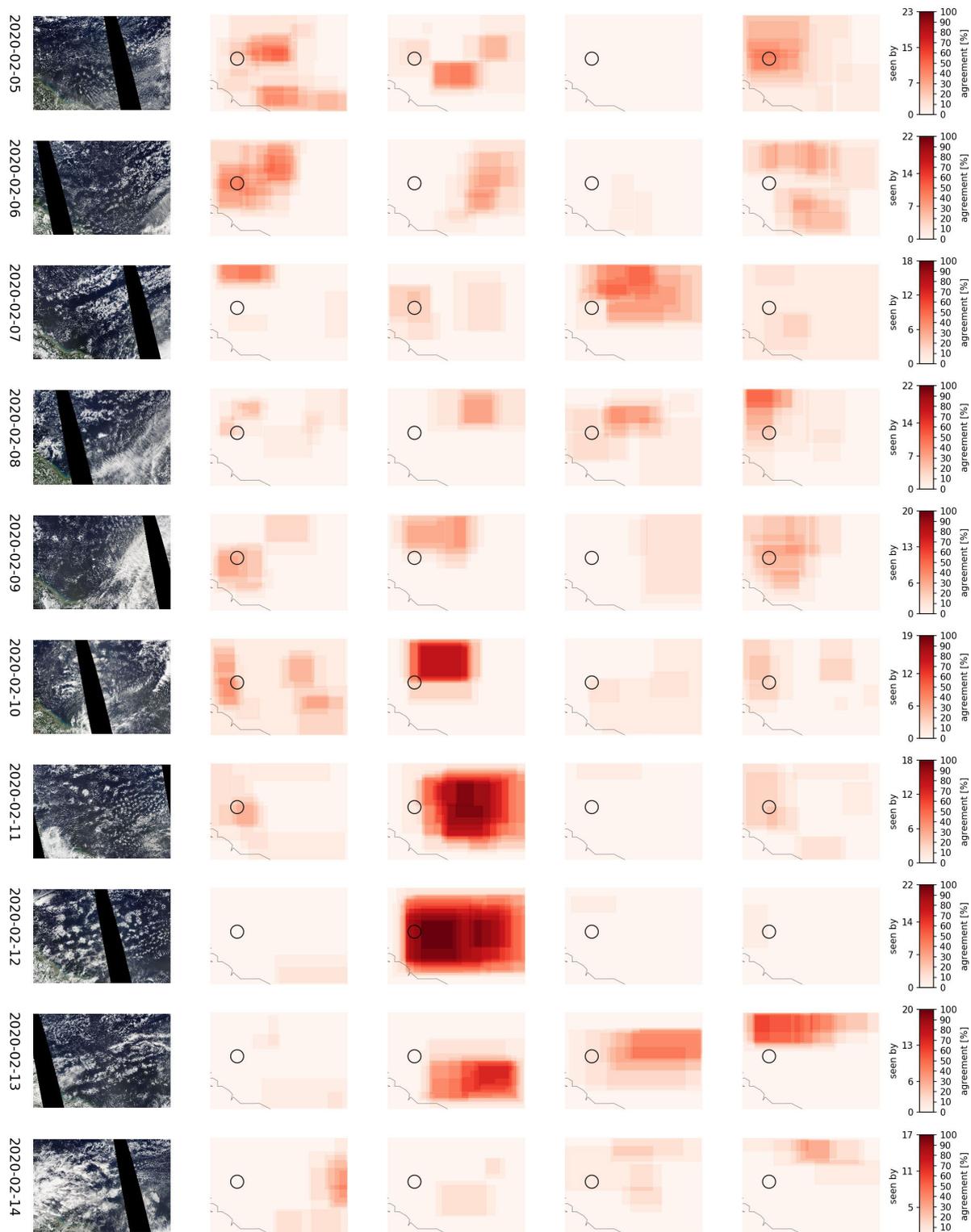
Figure A4. Continuation of Fig. A3
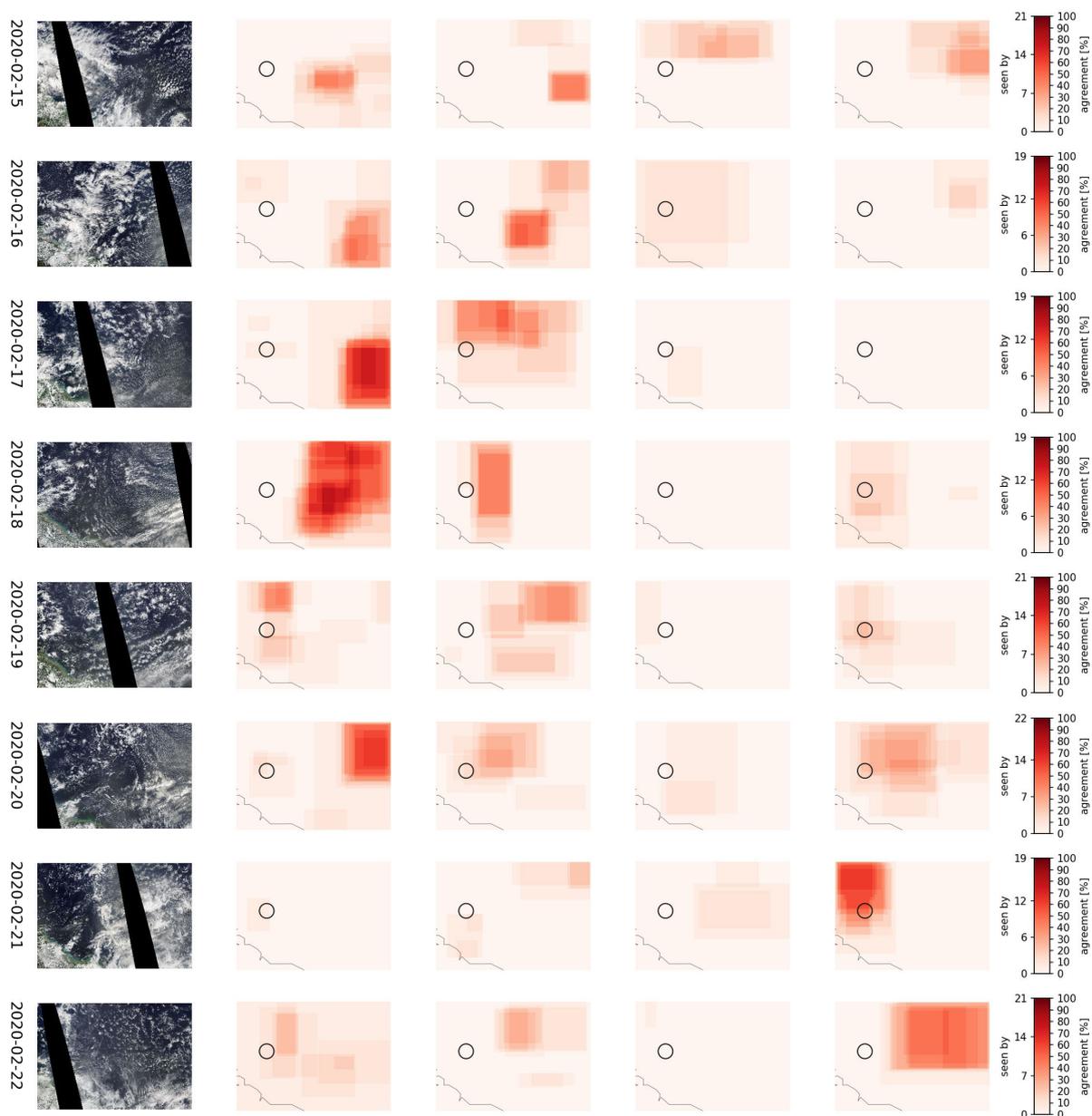
Figure A5. Continuation of Fig. A4
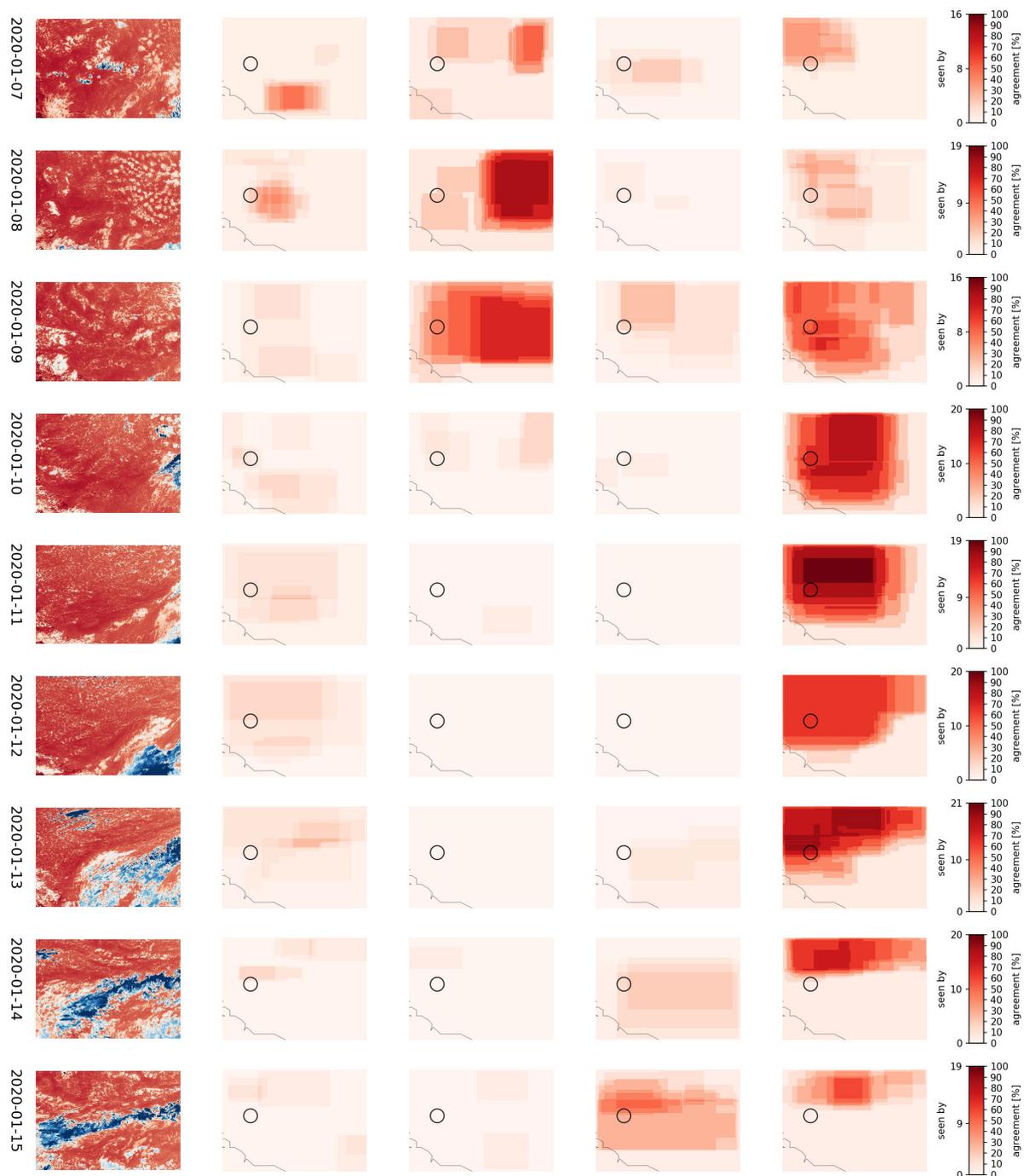
Figure A6. As Fig. A1 but for the infrared workflow. Images are showing the cloud field at 16 o'clock. (except 11.02.2020: 17 o'clock)
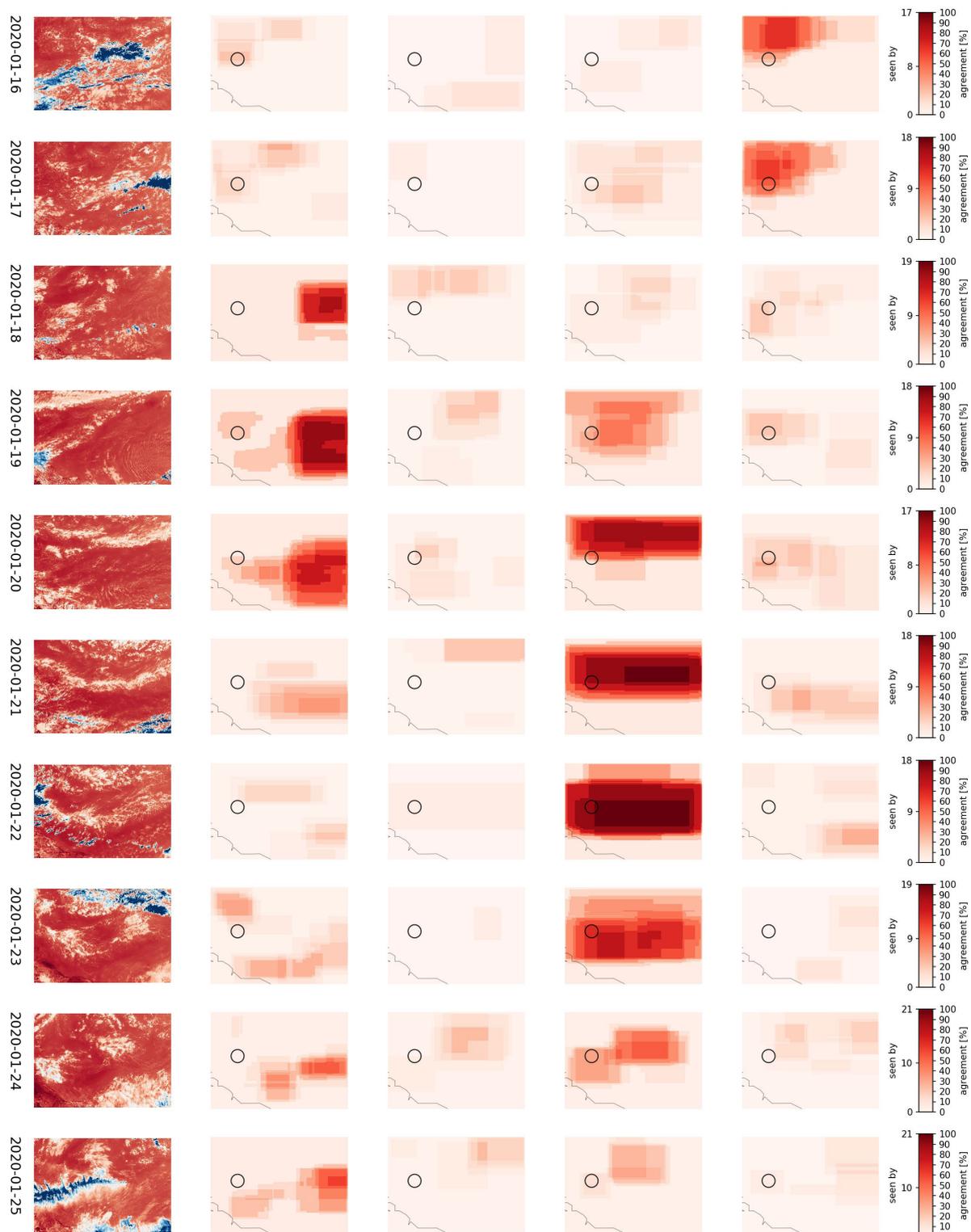
Figure A7. Continuation of Fig. A6
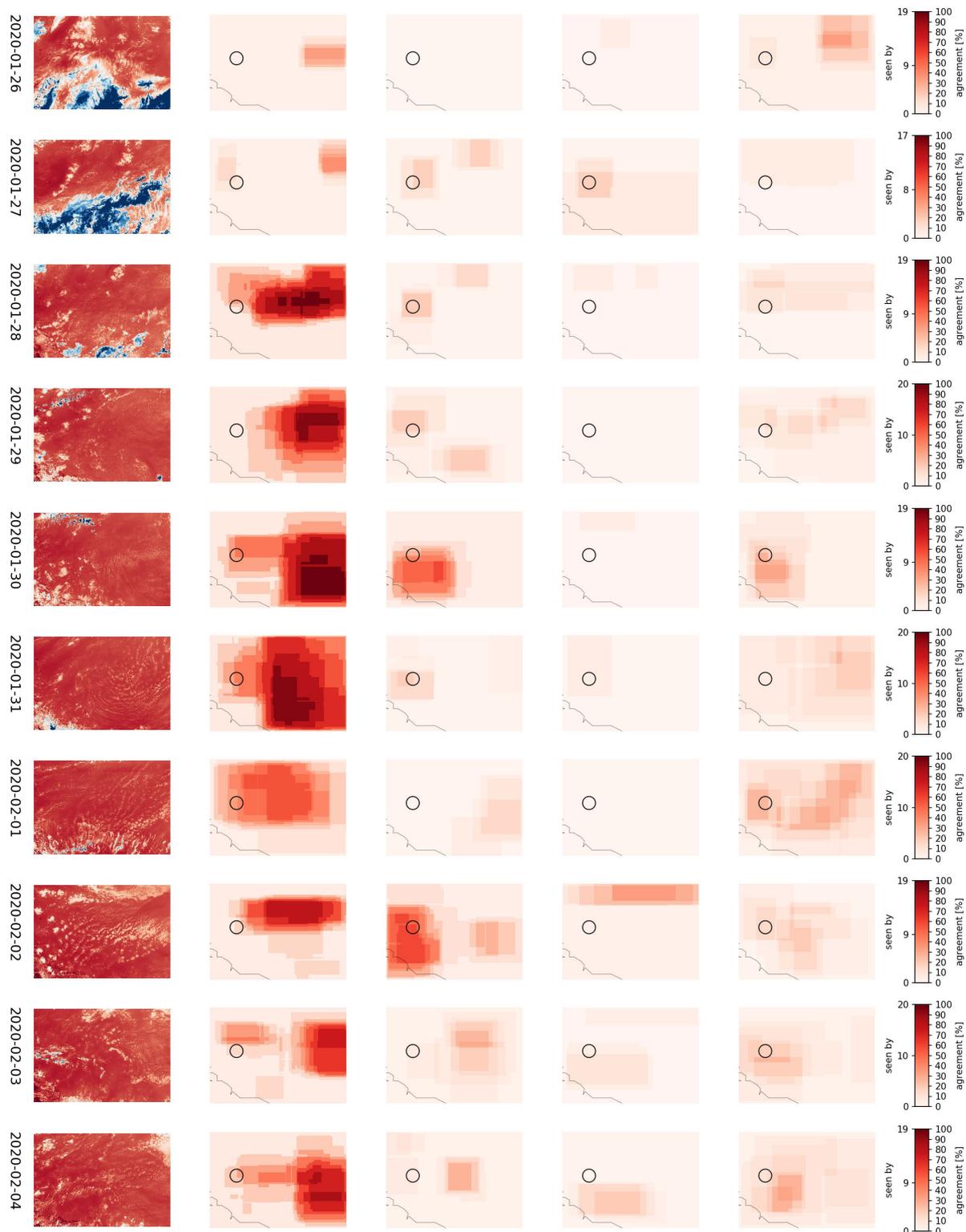
Figure A8. Continuation of Fig. A7
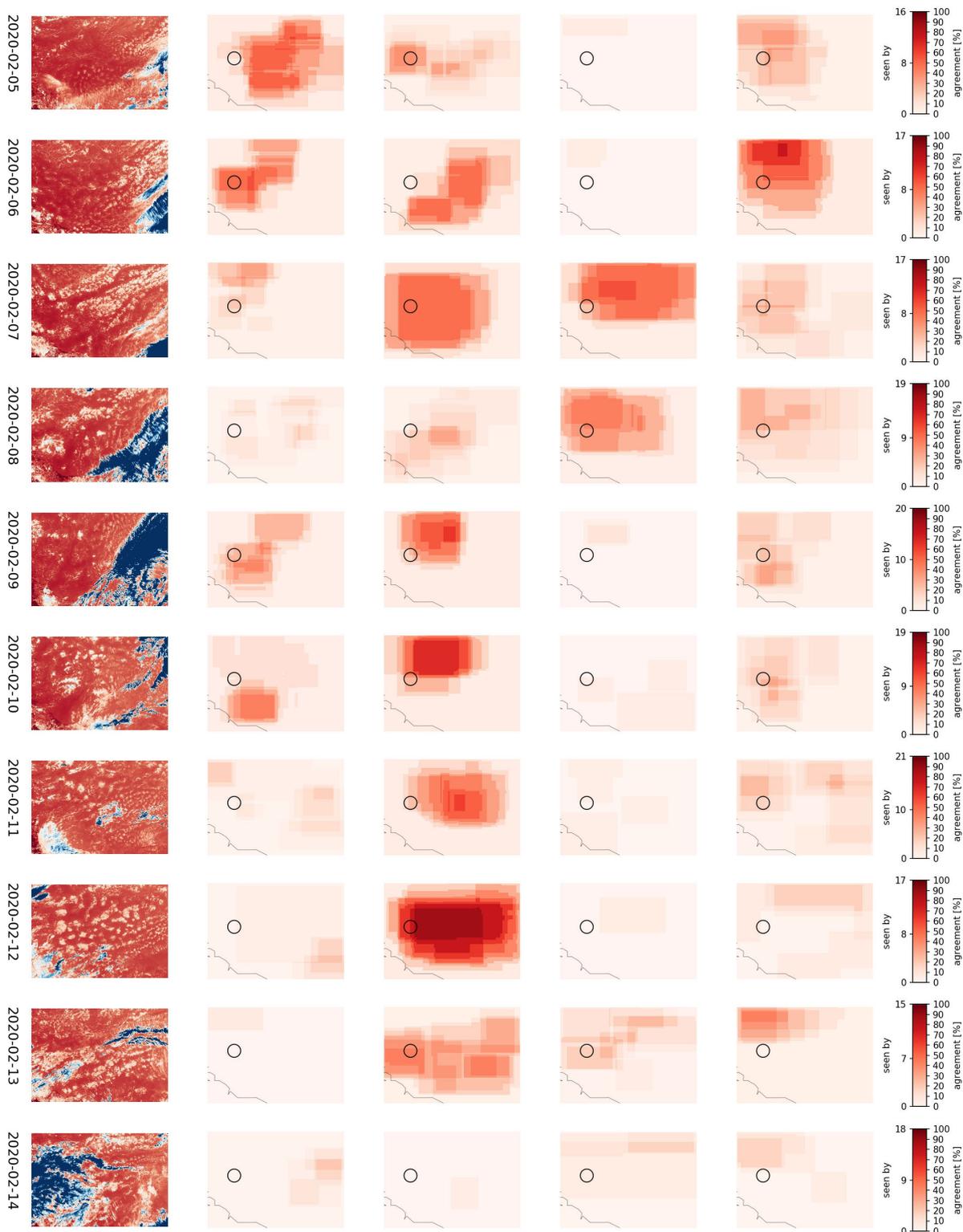
Figure A9. Continuation of Fig. A8
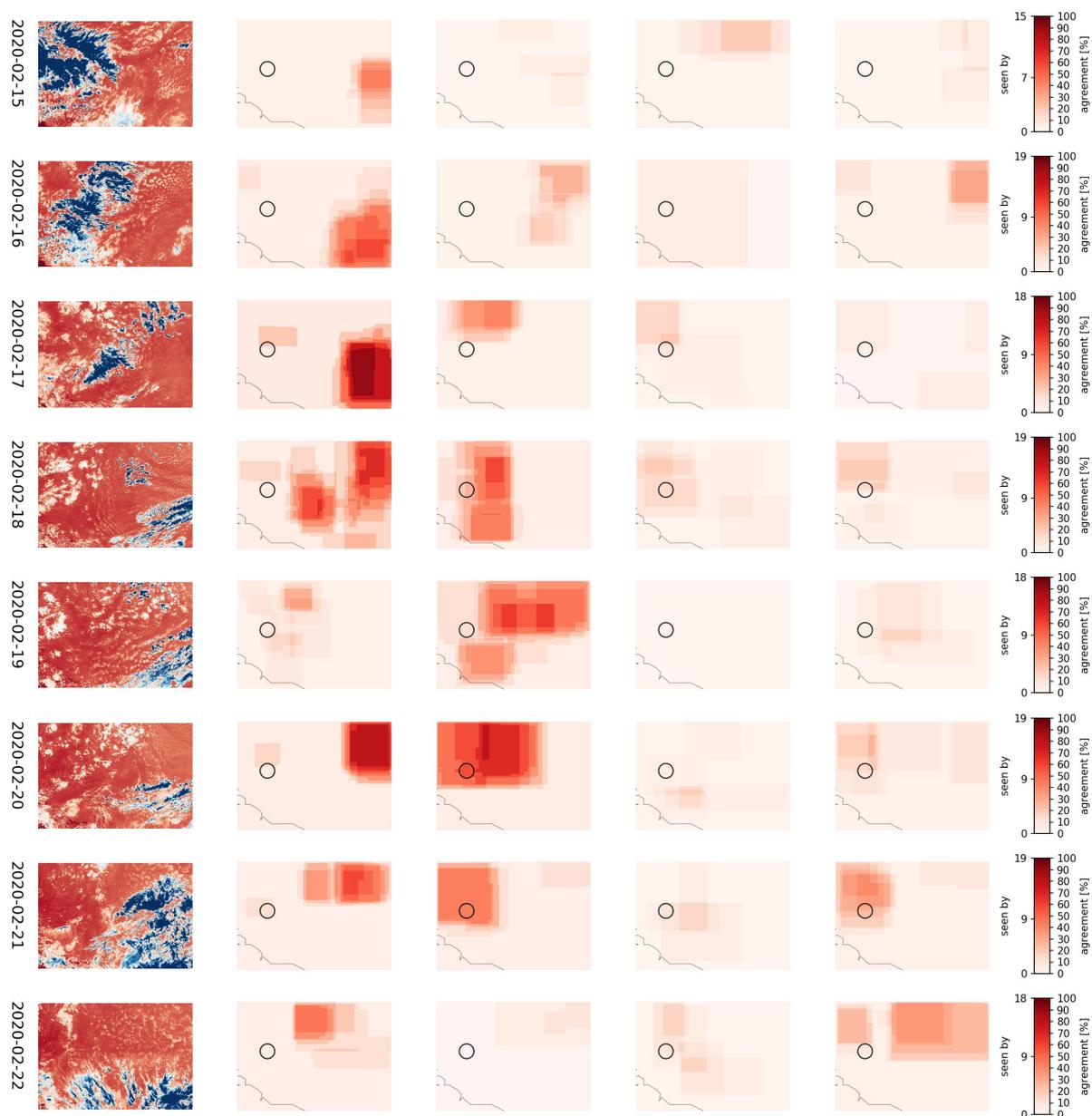
Figure A10. Continuation of Fig. A9
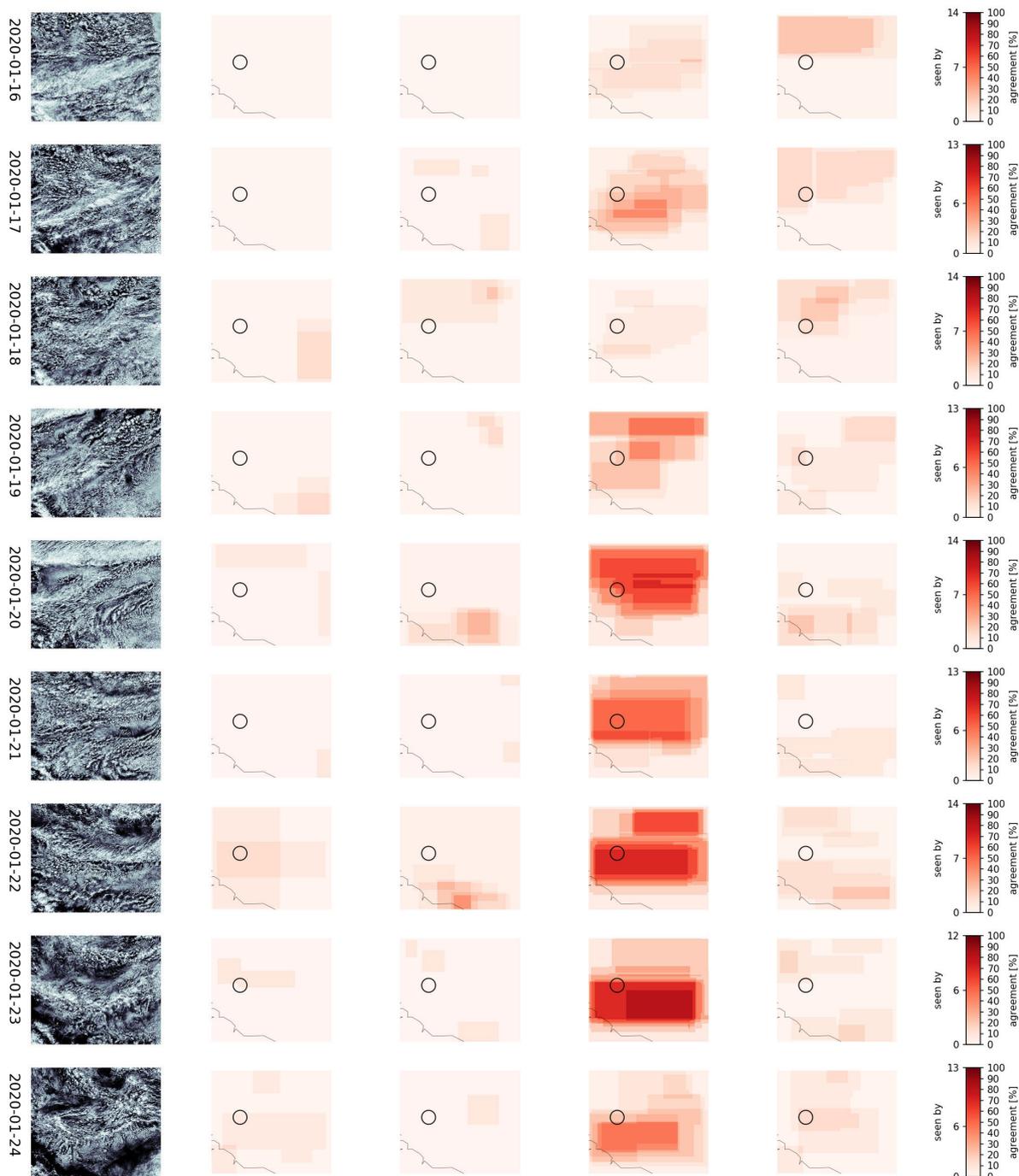
Figure A11. As Fig. A1 but for ICON albedo workflow. Images are showing the cloud field at midnight.
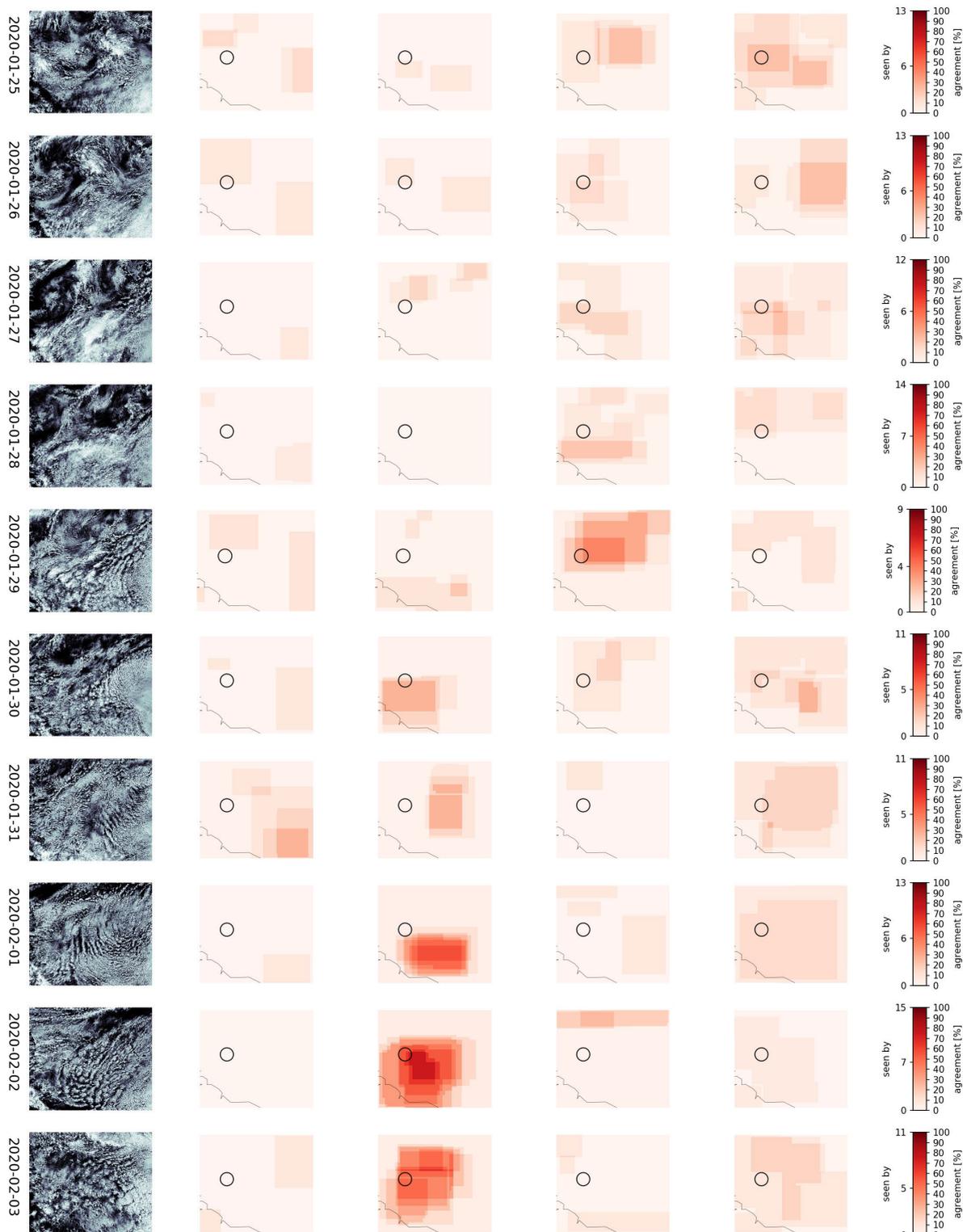
Figure A12. Continuation of Fig. A11
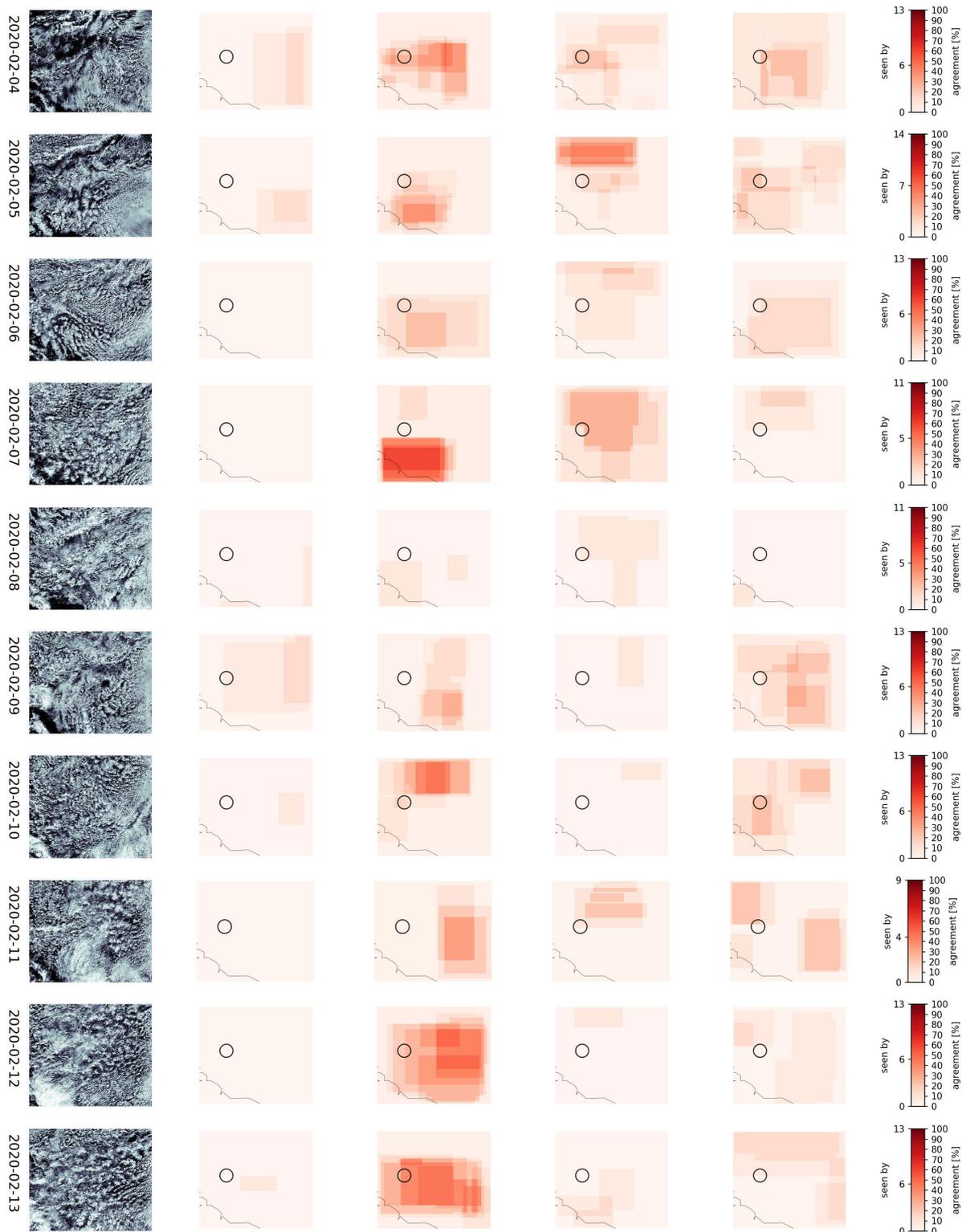
Figure A13. Continuation of Fig. A12
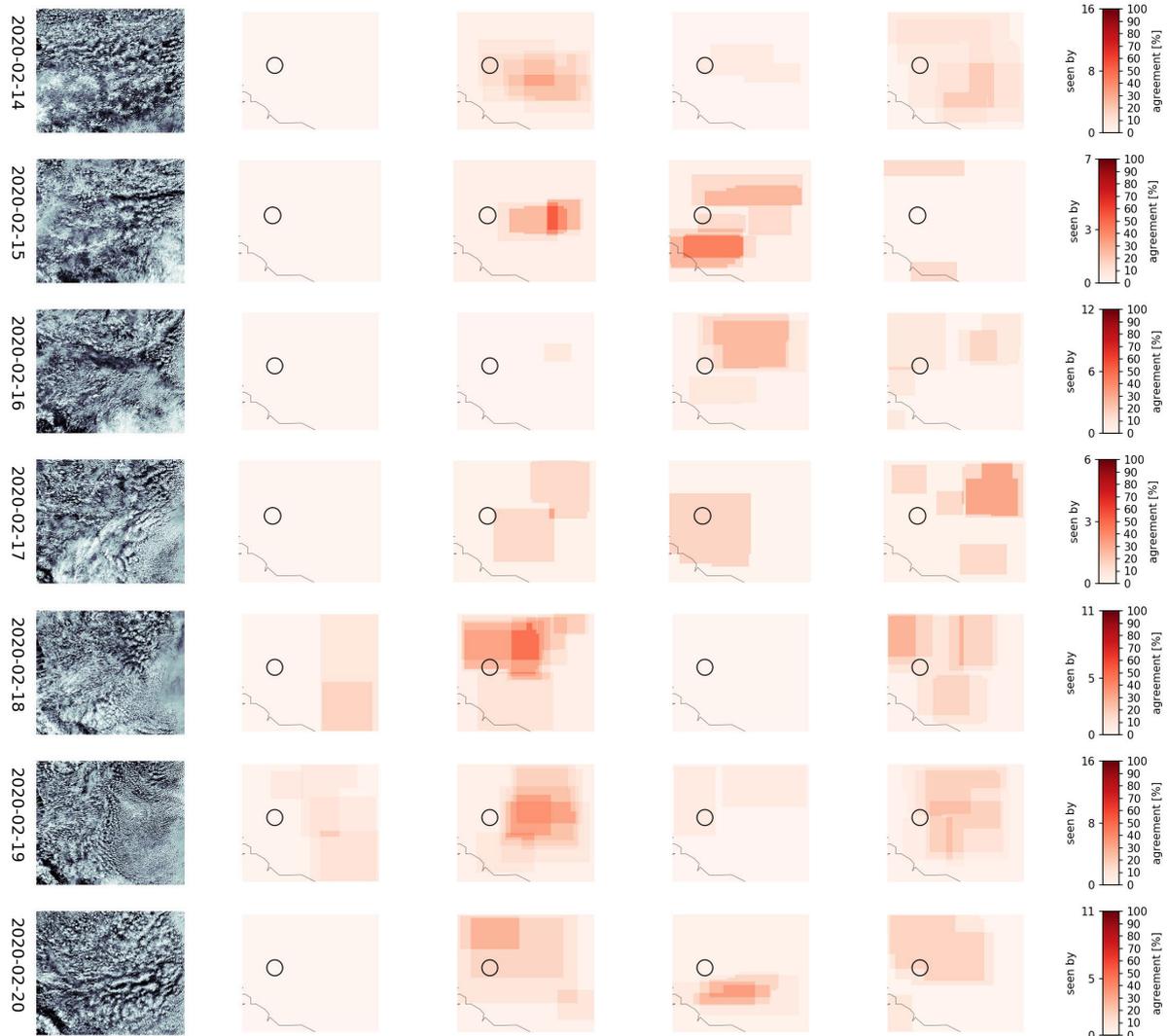
Figure A14. Continuation of Fig. A13

195 *Acknowledgements.* The author thanks the participants of the international remote classification event for their time in labeling the cloud patterns. Daniel Klocke is thanked for conducting the ICON-SRM simulations. Geet George is thanked for helpful feedback on an earlier version of this manuscript. We acknowledge the use of imagery from the NASA Worldview application (https://worldview.earthdata.nasa.gov), part of the NASA Earth Observing System Data and Information System (EOSDIS). GOES-16 Advanced Baseline Imager data is available at https://doi.org/10.7289/V5BV7DSR. Its Level 1b radiances were converted with Raspaud et al. (2019) to brightness temperatures.

200 This publication uses data generated via the Zooniverse.org platform, development of which is funded by generous support, including a Global Impact Award from Google, and by a grant from the Alfred P. Sloan Foundation.

References

Bony, S., Schulz, H., Vial, J., and Stevens, B.: Sugar, Gravel, Fish, and Flowers: Dependence of Mesoscale Patterns of Trade-Wind Clouds on Environmental Conditions, Geophysical Research Letters, 47, e2019GL085 988, https://doi.org/10.1029/2019GL085988, 2020.

205 Denby, L.: Discovering the Importance of Mesoscale Cloud Organization Through Unsupervised Classification, Geophysical Research Letters, 47, e2019GL085 190, https://doi.org/10.1029/2019GL085190, 2020.

European Organization For Nuclear Research and OpenAIRE: Zenodo, https://doi.org/10.25495/7GXK-RD71, 2013.

Konow, H., Ewald, F., George, G., Jacob, M., Klingebiel, M., Kölling, T., Luebke, A. E., Mieslinger, T., Pörtge, V., Radtke, J., Schäfer, M., Schulz, H., Vogel, R., Wirth, M., Bony, S., Crewell, S., Ehrlich, A., Forster, L., Giez, A., Gödde, F., Groß, S., Gutleben, M.,

210 Hagen, M., Hirsch, L., Jansen, F., Lang, T., Mayer, B., Mech, M., Prange, M., Schnitt, S., Vial, J., Walbröl, A., Wendisch, M., Wolf, K., Zinner, T., Zöger, M., Ament, F., and Stevens, B.: EUREC⁴A's HALO, Earth System Science Data Discussions, pp. 1–26, https://doi.org/10.5194/essd-2021-193, 2021.

Rasp, S., Schulz, H., Bony, S., and Stevens, B.: Combining Crowdsourcing and Deep Learning to Explore the Mesoscale Organization of Shallow Convection, Bulletin of the American Meteorological Society, 101, E1980–E1995, https://doi.org/10.1175/BAMS-D-19-0324.1,

215 2020.

Raspaud, M., Hoese, D., Lahtinen, P., Dybbroe, A., Finkensieper, S., Roberts, W., Rasmussen, L. Ø., Proud, S., Joro, S., Daruwala, R., Holl, G., Jasmin, T., BENR0, Leppelt, T., Egede, U., R.K.Garcia, Itkin, M., LTMeyer, Sigurðsson, E., Radar, S., Division, N., Aspenes, T., hazbottles, ColinDuff, joleenf, Cody, clementi, l., Honnorat, M., Schulz, H., Hatt, B., and Valentino, A.: Pytroll/Satpy: Version 0.16.0, Zenodo, https://doi.org/10.5281/zenodo.3250583, 2019.

220 Schulz, H.: C³ONTEXT: A Common Consensus on Convective OrgaNizaTion during the EUREC⁴A eXperimenT (Scripts), Zenodo, https://doi.org/10.5281/zenodo.5724762, 2021a.

Schulz, H.: C³ONTEXT: A Common Consensus on Convective OrgaNizaTion during the EUREC⁴A eXperimenT (Data), https://doi.org/10.5281/zenodo.5724585, 2021b.

Schulz, H., Eastman, R., and Stevens, B.: Characterization and Evolution of Organized Shallow Convection in the Downstream North Atlantic

225 Trades, Journal of Geophysical Research: Atmospheres, 126, e2021JD034 575, https://doi.org/10.1029/2021JD034575, 2021.

Siebert, H., Beals, M., Bethke, J., Bierwirth, E., Conrath, T., Dieckmann, K., Ditas, F., Ehrlich, A., Farrell, D., Hartmann, S., Izaguirre, M. A., Katzwinkel, J., Nuijens, L., Roberts, G., Schäfer, M., Shaw, R. A., Schmeissner, T., Serikov, I., Stevens, B., Stratmann, F., Wehner, B., Wendisch, M., Werner, F., and Wex, H.: The Fine-Scale Structure of the Trade Wind Cumuli over Barbados – an Introduction to the CARRIBA Project, Atmospheric Chemistry and Physics, 13, 10 061–10 077, https://doi.org/10.5194/acp-13-10061-2013, 2013.

230 Stevens, B., Bony, S., Brogniez, H., Hentgen, L., Hohenegger, C., Kiemle, C., L'Ecuyer, T. S., Naumann, A. K., Schulz, H., Siebesma, P. A., Vial, J., Winker, D. M., and Zuidema, P.: Sugar, Gravel, Fish and Flowers: Mesoscale Cloud Patterns in the Trade Winds, Quarterly Journal of the Royal Meteorological Society, 146, 141–152, https://doi.org/10.1002/qj.3662, 2020.

Stevens, B., Bony, S., Farrell, D., Ament, F., Blyth, A., Fairall, C., Karstensen, J., Quinn, P. K., Speich, S., Acquistapace, C., Aemisegger, F., Albright, A. L., Bellenger, H., Bodenschatz, E., Caesar, K.-A., Chewitt-Lucas, R., de Boer, G., Delanoë, J., Denby, L., Ewald, F., Fildier,

235 B., Forde, M., George, G., Gross, S., Hagen, M., Hausold, A., Heywood, K. J., Hirsch, L., Jacob, M., Jansen, F., Kinne, S., Klocke, D., Kölling, T., Konow, H., Lothon, M., Mohr, W., Naumann, A. K., Nuijens, L., Olivier, L., Pincus, R., Pöhlker, M., Reverdin, G., Roberts, G., Schnitt, S., Schulz, H., Siebesma, A. P., Stephan, C. C., Sullivan, P., Touzé-Peiffer, L., Vial, J., Vogel, R., Zuidema, P., Alexander, N., Alves, L., Arixi, S., Asmath, H., Bagheri, G., Baier, K., Bailey, A., Baranowski, D., Baron, A., Barrau, S., Barrett, P. A., Batier,

F., Behrendt, A., Bendinger, A., Beucher, F., Bigorre, S., Blades, E., Blossey, P., Bock, O., Böing, S., Bosser, P., Bourras, D., Bouruet-Aubertot, P., Bower, K., Branellec, P., Branger, H., Brennek, M., Brewer, A., Brilouet, P.-E., Brügmann, B., Buehler, S. A., Burke, E., Burton, R., Calmer, R., Canonici, J.-C., Carton, X., Cato Jr., G., Charles, J. A., Chazette, P., Chen, Y., Chilinski, M. T., Choularton, T., Chuang, P., Clarke, S., Coe, H., Cornet, C., Coutris, P., Couvreux, F., Crewell, S., Cronin, T., Cui, Z., Cuypers, Y., Daley, A., Damerell, G. M., Dauhut, T., Deneke, H., Desbios, J.-P., Dörner, S., Donner, S., Douet, V., Drushka, K., Dütsch, M., Ehrlich, A., Emanuel, K., Emmanouilidis, A., Etienne, J.-C., Etienne-Leblanc, S., Faure, G., Feingold, G., Ferrero, L., Fix, A., Flamant, C., Flatau, P. J., Foltz, G. R., Forster, L., Furtuna, I., Gadian, A., Galewsky, J., Gallagher, M., Gallimore, P., Gaston, C., Gentemann, C., Geyskens, N., Giez, A., Gollop, J., Gouirand, I., Gourbeyre, C., de Graaf, D., de Groot, G. E., Grosz, R., Güttler, J., Gutleben, M., Hall, K., Harris, G., Helfer, K. C., Henze, D., Herbert, C., Holanda, B., Ibanez-Landeta, A., Intrieri, J., Iyer, S., Julien, F., Kalesse, H., Kazil, J., Kellman, A., Kidane, A. T., Kirchner, U., Klingebiel, M., Körner, M., Kremper, L. A., Kretzschmar, J., Krüger, O., Kumala, W., Kurz, A., L'Hégaret, P., Labaste, M., Lachlan-Cope, T., Laing, A., Landschützer, P., Lang, T., Lange, D., Lange, I., Laplace, C., Lavik, G., Laxenaire, R., Le Bihan, C., Leandro, M., Lefevre, N., Lena, M., Lenschow, D., Li, Q., Lloyd, G., Los, S., Losi, N., Lovell, O., Luneau, C., Makuch, P., Malinowski, S., Manta, G., Marinou, E., Marsden, N., Masson, S., Maury, N., Mayer, B., Mayers-Als, M., Mazel, C., McGeary, W., McWilliams, J. C., Mech, M., Mehlmann, M., Meroni, A. N., Mieslinger, T., Minikin, A., Minnett, P., Möller, G., Morfa Avalos, Y., Muller, C., Musat, I., Napoli, A., Neuberger, A., Noisel, C., Noone, D., Nordsiek, F., Nowak, J. L., Oswald, L., Parker, D. J., Peck, C., Person, R., Philippi, M., Plueddemann, A., Pöhlker, C., Pörtge, V., Pöschl, U., Pologne, L., Posyniak, M., Prange, M., Quiñones Meléndez, E., Radtke, J., Ramage, K., Reimann, J., Renault, L., Reus, K., Reyes, A., Ribbe, J., Ringel, M., Ritschel, M., Rocha, C. B., Rochetin, N., Röttenbacher, J., Rollo, C., Royer, H., Sadoulet, P., Saffin, L., Sandiford, S., Sandu, I., Schäfer, M., Schemann, V., Schirmacher, I., Schlenczek, O., Schmidt, J., Schröder, M., Schwarzenboeck, A., Sealy, A., Senff, C. J., Serikov, I., Shohan, S., Siddle, E., Smirnov, A., Späth, F., Spooner, B., Stolla, M. K., Szkółka, W., de Szoeke, S. P., Tarot, S., Tetoni, E., Thompson, E., Thomson, J., Tomassini, L., Totems, J., Ubele, A. A., Villiger, L., von Arx, J., Wagner, T., Walther, A., Webber, B., Wendisch, M., Whitehall, S., Wiltshire, A., Wing, A. A., Wirth, M., Wiskandt, J., Wolf, K., Worbes, L., Wright, E., Wulfmeyer, V., Young, S., Zhang, C., Zhang, D., Ziemen, F., Zinner, T., and Zöger, M.: EUREC^{4}A, Earth System Science Data, 13, 4067–4119, https://doi.org/10.5194/essd-13-4067-2021, 2021.

Tompkins Adrian M. and Semie Addisu G.: Organization of Tropical Convection in Low Vertical Wind Shears: Role of Updraft Entrainment, Journal of Advances in Modeling Earth Systems, 9, 1046–1068, https://doi.org/10.1002/2016MS000802, 2017.

Vial, J., Vogel, R., and Schulz, H.: On the Daily Cycle of Mesoscale Cloud Organization in the Winter Trades, Quarterly Journal of the Royal Meteorological Society, 147, 2850–2873, https://doi.org/10.1002/qj.4103, 2021.

Wessel, P. and Smith, W. H. F.: A Global, Self-Consistent, Hierarchical, High-Resolution Shoreline Database, Journal of Geophysical Research: Solid Earth, 101, 8741–8743, https://doi.org/10.1029/96JB00104, 1996.

Wood, R. and Hartmann, D. L.: Spatial Variability of Liquid Water Path in Marine Low Cloud: The Importance of Mesoscale Cellular Convection, Journal of Climate, 19, 1748–1764, https://doi.org/10.1175/JCLI3702.1, 2006.

Zhang, Y., Stevens, B., and Ghil, M.: On the Diurnal Cycle and Susceptibility to Aerosol Concentration in a Stratocumulus-Topped Mixed Layer, Quarterly Journal of the Royal Meteorological Society, 131, 1567–1583, https://doi.org/10.1256/qj.04.103, 2005.